Contrasting Effects of the Persistent Na$^+$ Current on Neuronal Excitability and Spike Timing

Koen Vervaeke,[1,2,4] Hua Hu,[1,2,4] Lyle J. Graham,[3] and Johan F. Storm[1,2,*]
[1] Department of Physiology
Institute of Basal Medicine
[2] Centre for Molecular Biology and Neuroscience
University of Oslo
PB 1103 Blindern
N-0317 Oslo
Norway
[3] Laboratory of Neurophysics and Physiology
CNRS UMR 8119
UFR Biomedicale de l'Universite Rene Descartes
45 rue des Saints-Peres
75006 Paris
France

Summary

The persistent Na$^+$ current, I_{NaP}, is known to amplify subthreshold oscillations and synaptic potentials, but its impact on action potential generation remains enigmatic. Using computational modeling, whole-cell recording, and dynamic clamp of CA1 hippocampal pyramidal cells in brain slices, we examined how I_{NaP} changes the transduction of excitatory current into action potentials. Model simulations predicted that I_{NaP} increases afterhyperpolarizations, and, although it increases excitability by reducing rheobase, I_{NaP} also reduces the gain in discharge frequency in response to depolarizing current (f/I gain). These predictions were experimentally confirmed by using dynamic clamp, thus circumventing the longstanding problem that I_{NaP} cannot be selectively blocked. Furthermore, we found that I_{NaP} increased firing regularity in response to sustained depolarization, although it decreased spike time precision in response to single evoked EPSPs. Finally, model simulations demonstrated that I_{NaP} increased the relative refractory period and decreased interspike-interval variability under conditions resembling an active network in vivo.

Introduction

Neurons transduce synaptic input into action potentials through interplay between the large ionic membrane currents underlying the action potential and a set of smaller currents operating at membrane potentials just below the spike threshold. The latter "threshold currents" are pivotal for determining spike timing, spike pattern, and frequency. Determining the roles of these currents is therefore essential for understanding how neurons encode information into a pattern of action potentials.

The persistent sodium current (I_{NaP}) is a threshold current prominently expressed in neocortical and hippo-

campal pyramidal neurons (Stafstrom et al., 1985; French and Gage, 1985) and many other mammalian neurons (Crill, 1996). Both I_{NaP} and the classical spike-generating transient Na$^+$ current (I_{NaT}) activate rapidly. I_{NaP} differs from I_{NaT} both by lacking fast inactivation and by activating at more negative potentials, ~10 mV below the spike threshold. In accordance with these features, I_{NaP} has been reported to modulate subthreshold dynamics. We recently showed that I_{NaP} contributes to subthreshold electrical resonance in the theta frequency range in hippocampal pyramidal neurons (Hu et al., 2002). I_{NaP} has also been shown to enhance excitatory and inhibitory postsynaptic potentials in hippocampal (Lipowsky et al., 1996) and neocortical pyramidal cells (Stafstrom et al., 1985; Stuart and Sakmann, 1995; Stuart, 1999).

Various aspects of how a neuron translates synaptic input into spike frequency—so-called current-to-frequency transduction—can be studied by injecting a depolarizing current (I) into the cell and plotting the spike frequency (f) as a function of the current intensity (f/I plot) (Lanthorn et al., 1984). A major mechanism controlling the f/I relation is the afterhyperpolarizations (AHPs) that follow action potentials (Vogalis et al., 2003). Being due mainly to opening of K$^+$ channels triggered by spike depolarization or by associated influx of Ca^{2+}, AHP conductances control the firing frequency, regularity, and spike timing precision in a variety of neurons, including hippocampal pyramidal cells (Hotson and Prince, 1980; Madison and Nicoll, 1984; Storm, 1989). Through both direct hyperpolarization and an increase in the membrane conductance, AHPs contribute to the relative refractory period, thus mediating negative-feedback regulation of the discharge frequency.

Activation of an inward current such as I_{NaP} is at least expected to increase neuronal excitability. Since I_{NaP} can act as an intrinsic amplification mechanism of subthreshold voltage perturbations (Crill, 1996), we hypothesized that it might also affect the dynamics of AHPs and indirectly modify the input-output relations of the cell. Since AHPs have been suggested to improve temporal precision during spike trains (de Ruyter van Steveninck et al., 1997; Berry and Meister, 1998) and promote stable rhythmic spiking by filtering out noise (Schreiber et al., 2004), we also wished to determine how I_{NaP} affects spike timing and regularity. Hippocampal CA1 pyramidal cells are a convenient prototype for testing these ideas, in particular since their AHPs have been characterized in multiple previous studies. In this cell type, spikes are followed by three types of AHPs due to different K$^+$ channels: fast (fAHP), medium (mAHP), and slow (sAHP) (Storm, 1990), a pattern which is found in a variety of mammalian neurons.

To date, technical difficulties have precluded direct testing of the impact of I_{NaP} on neuronal firing behavior and the f/I relation. While the roles of other threshold currents have been studied with specific pharmacological or genetic manipulations (e.g., Nolan et al., 2003; Peters et al., 2005), such approaches are hampered in the case of I_{NaP} because of its close relationship with

*Correspondence: jstorm@medisin.uio.no
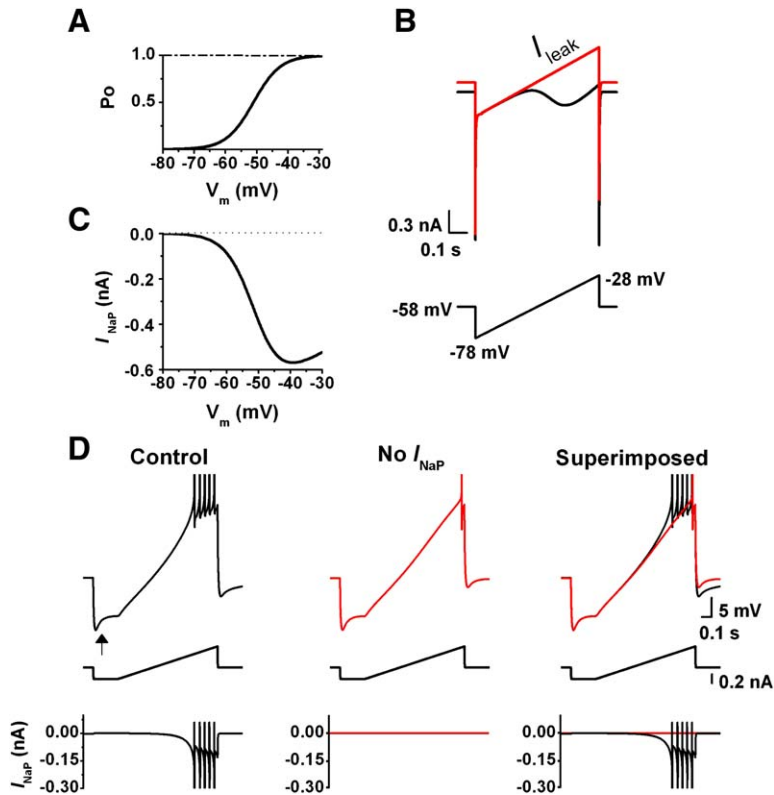[4] These authors contributed equally to this work.

Figure 1. Model Simulations of I_{NaP} Behavior under Voltage and Current Clamp

(A) Steady-state activation curve of I_{NaP} model. P_o is the open probability. The voltage-independent activation and deactivation time constant was 1 ms.

(B) I_{NaP} (black) compared to leak current (red) in response to a voltage ramp command (lower trace) in the model.

(C) I_{NaP} obtained by subtracting the current responses shown in (B).

(D) Voltage responses (upper panels) to a current ramp command (middle panels: −0.25 to +0.45 nA in 1 s; V_{rest} was −75 mV) with (black) and without I_{NaP} (red). I_{NaP} is shown in bottom panels.

I_{NaT}. In particular, blockers of I_{NaP} (e.g., TTX and phenytoin) also affect the I_{NaT}-dependent action potentials, possibly because I_{NaP} and I_{NaT} arise from different gating modes of the same channel type (Alzheimer et al., 1993; Crill, 1996).

In this study, we circumvent these difficulties by combining computational modeling with dynamic-clamp electrophysiological measurements. First, we tested our ideas theoretically. Simulations revealed that I_{NaP} not only enhanced AHPs, it also had contrasting effects on excitability. On one hand, and as expected, I_{NaP} reduced the minimal current necessary to evoke spiking (rheobase). On the other hand, I_{NaP} also reduced the slope (gain) of the f/I relation. We then tested these predictions experimentally in whole-cell recordings from rat CA1 pyramidal neurons by using dynamic clamp to selectively eliminate I_{NaP} or to artificially restore I_{NaP} in the presence of TTX. These experiments not only confirmed the model predictions, they also showed additional and contrasting effects of I_{NaP} on the temporal aspects of spike firing. On one hand, I_{NaP} increased the regularity of repetitive firing in response to sustained depolarization, but on the other hand, I_{NaP} also decreased spike time precision in response to single EPSPs. Thus, I_{NaP} was shown to have contrasting effects on both different indexes of excitability (rheobase and f/I gain) and different indexes of spike timing accuracy (firing regularity during repetitive firing and spike time precision during transient synaptic excitation). In addition, model simulations demonstrated that I_{NaP} increased the relative refractory period and decreased interspike-interval variability under conditions resembling an active network in vivo.

Results

Model simulations were generally performed first to predict the outcome of future experiments; these predictions were subsequently tested by electrophysiological recordings in brain slices. Thus, the model predictions illustrated in both Figures 1 and 3 were made before testing them experimentally, as shown in Figures 2 and 4. Next, the model predictions illustrated in Figure 5A were performed, followed by the experimental tests shown in Figures 5B–5C. Once the main (qualitative) predictions had been made, tested, and confirmed, data from the experiments were sometimes used for adjusting the parameters of the model to achieve a better quantitative fit to the data.

Developing the CA1 Pyramidal Model

As a first approach to determining whether I_{NaP} can affect AHPs, we performed numerical simulations using a computer model of a rat CA1 pyramidal neuron derived from a previous model (Borg-Graham, 1999). Our model is described in detail in Experimental Procedures (Computational Methods) and in the Supplemental Data available with this article online. Briefly, it is a compartmental model consisting of a dendritic cable and a soma with 11 active membrane conductances and intracellular Ca^{2+} dynamics. This model reproduces quite accurately the spiking behavior, AHPs, and resonance properties of these neurons (Shao et al., 1999; Hu et al., 2002; Gu et al., 2005).

For this study, we took special care to accurately model the Na^+ conductances. In the original model (Borg-Graham, 1999), a novel four-state Markov model
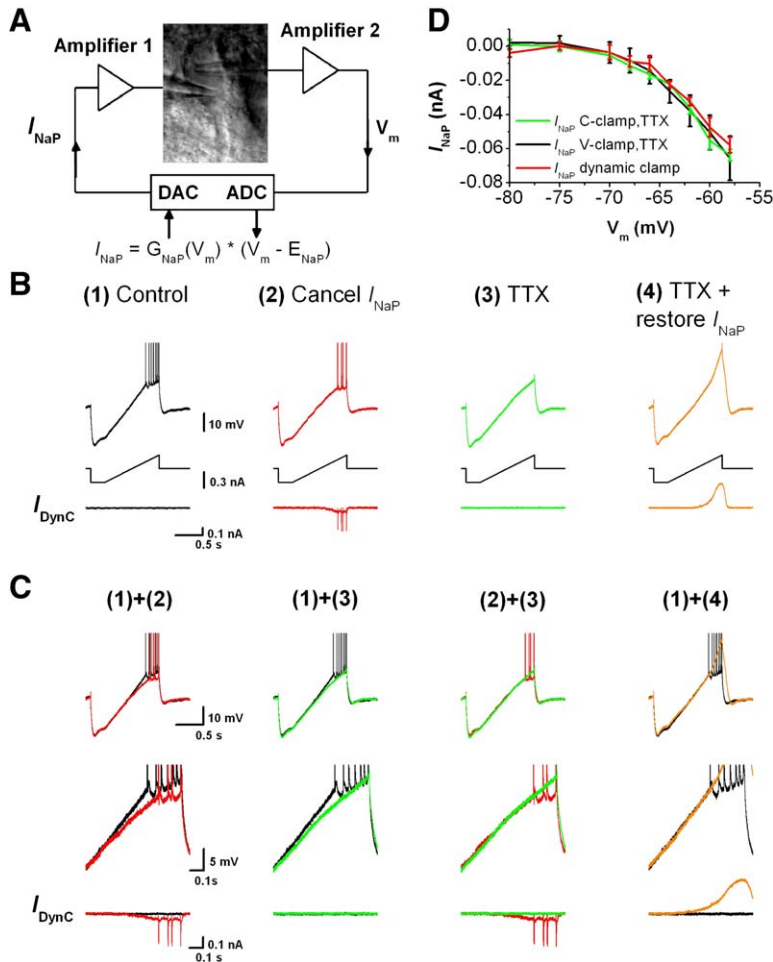
Figure 2. Electrophysiological Analysis of I_{NaP} Behavior with TTX and Dynamic Clamp

(A) Diagram of the experimental setup with dynamic clamp. Dual whole-cell configuration at the soma was established with two patch pipettes: one for voltage recording and the other for current injection. The simulated I_{NaP} was calculated by the dynamic-clamp software from the measured membrane potential V_m and injected into the neuron in real time. To cancel the intrinsic I_{NaP} generated by the neuron, a negative current equal to the simulated I_{NaP} was injected into the cell, whereas a positive current equal to the simulated I_{NaP} was injected to restore I_{NaP} in the presence of TTX.

(B) Representative traces showing the voltage response to a current ramp (-0.25 to $+0.25$ nA) before (1) and after (2) canceling I_{NaP} with dynamic clamp, followed by application of 1 μM TTX and dynamic clamp turned off (3) and after restoring I_{NaP} with dynamic clamp in the presence of TTX (4). These four conditions were executed in sequence in each cell (n = 5). Before the start of each protocol, the cell was maintained at -70 mV by steady-current injection. The bottom traces in (B) and (C) show the current output from the dynamic clamp (I_{DynC}) for each condition.

(C) The same traces as in (B) shown superimposed and on expanded scales.

(D) Voltage dependence of I_{NaP}. Summary plots from three types of measurements: (1) the subthreshold TTX-sensitive current obtained in voltage clamp (*V-clamp, TTX*; n = 8), (2) the TTX-sensitive subthreshold current obtained from current clamp recordings as in (B) (*C-clamp, TTX*; n = 5) and (3) I_{NaP} produced by dynamic clamp (n = 5).

of the entire Na^+ current was used in order to better replicate the dynamic and steady-state behavior of this current. In particular, the steady-state component of this I_{Na} model is consistent with reported measurements of I_{NaP} (French et al., 1990), which in turn is much less than the window current of Hodgkin-Huxley-type models of I_{Na} (Traub et al., 1994; Migliore et al., 1999). Furthermore, the steady-state and dynamic components of the Markov I_{Na} model can be adjusted relatively independently. For clarity, therefore, we here use I_{NaT} and I_{NaP} as two separate entities modeled as a Markov model (based on the Borg-Graham [1999] I_{Na} model, but without a steady-state component) and a Hodgkin-Huxley model, respectively.

**Modeling the Persistent Na^+ Current, I_{NaP}**

Using the cell model, we studied I_{NaP} in both voltage- and current-clamp simulations (Figure 1). The steady-state activation curve (Figure 1A) and the maximum conductance of the I_{NaP} model were based on our previous voltage-clamp measurements in CA1 pyramidal neurons (Hu et al., 2002) and agree well with other experimental reports (French et al., 1990). A simulated depolarizing voltage ramp (Figure 1B, lower panel) produced an I_{NaP} (Figures 1B and 1C) that agreed well with experimental results (see Figure 2A in French et al., 1990 and Figure 5E in Hu et al., 2002). Only indirect indications of the I_{NaP} activation and deactivation kinetics are avail-

able because I_{NaT} obstructs detailed voltage-clamp analysis. Nevertheless, at subthreshold potentials, which is the range of greatest interest to our study, I_{NaP} has been shown to activate and deactivate within the settling time of single-electrode voltage clamp, i.e., in <3–4 ms (Stafstrom et al., 1985; French et al., 1990; Crill, 1996; Kay et al., 1998; Taddese and Bean, 2002) (see also Figure S2). In the model, we tested various voltage-independent time constants ranging from 0.5 to 10 ms and found that these variations made no qualitative difference to our results (data not shown), except where explicitly stated (see Figure 8).

Some authors have reported a slow inactivation of I_{NaP}, with a time constant of several seconds (French et al., 1990; Magistretti and Alonso, 1999). Therefore, we checked whether such inactivation would affect our results by including an additional inactivation particle based on the Hodgkin-Huxley description from Magistretti and Alonso (1999). However, slow inactivation of I_{NaP} did not qualitatively affect our results (data not shown); therefore, we performed all subsequent simulations with the simplest Hodgkin-Huxley model with only a single activation particle and no inactivation.

Prediction from Modeling: I_{NaP} Alters the Response to a Current Ramp

To test how I_{NaP} behaves in current clamp, we simulated the injection of a depolarizing-current ramp (Figure 1D).

A

B
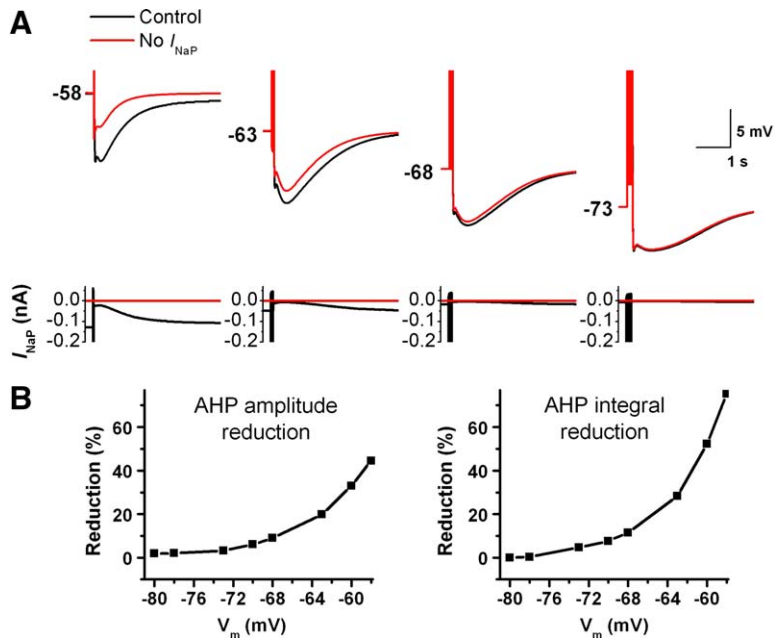
Figure 3. Model Simulations Showing Voltage-Dependent Amplification of AHPs

(A) AHPs evoked by a train of spikes, at different holding potentials (maintained by steady-current injection), before (black) and after (red) removing I_{NaP}. Each action potential was triggered by a brief current pulse (1 ms, 2 nA at 50 Hz), and the spike number was adjusted to yield AHPs of approximately constant amplitude for all holding potentials (although this could not be fully achieved at hyperpolarized potentials). The I_{NaP} response is shown at the bottom.

(B) AHP peak amplitude reduction (left panel) and AHP integral reduction (right) at different holding potentials. The AHP integral was calculated as the area between the AHP and the holding potential, between 0 and 5000 ms after the last spike. (For holding currents with and without I_{NaP} and the number of evoked spikes at each holding potential, see Tables S1 and S2).

The negative-current step before the start of the ramp evoked a "sag" (arrow) due to the activation of the h current, I_h (Halliwell and Adams, 1982). When I_{NaP} was omitted from the model (Figure 1D, middle), the depolarizing slope beyond ~ -65 mV decreased (Figure 1D, right), in agreement with experimental data (Hotson et al., 1979), and the spiking was reduced. The bottom panels of Figure 1D show I_{NaP} during these simulations.

Experimental Test: I_{NaP} Can Be Accurately Canceled by Dynamic Clamp

We next tested these theoretical predictions by recording from CA1 pyramidal cells in hippocampal slices using two approaches: (1) blockade of I_{NaP} with tetrodotoxin (TTX) and (2) electrical cancellation and addition of I_{NaP} by dynamic clamp.

The dynamic-clamp technique was used to cancel I_{NaP} without affecting I_{NaT}. To this end, we used the I_{NaP} kinetics of our pyramidal-cell model in the dynamic clamp (Figure 2A). Available evidence suggests that I_{NaP} in CA1 and neocortical pyramidal neurons is mostly of perisomatic origin (French et al., 1990; Stuart and Sakmann, 1995; Andreasen and Lambert, 1999). Therefore, space clamp limitations are unlikely to substantially affect our results (see also Supplemental Data).

Like in the model simulations, we injected a negative-current step followed by a depolarizing-current ramp and observed a similar "I_h sag" (Figures 2B and 2C) (n = 5). The bottom panels in Figures 2B and 2C show the simulated I_{NaP} that was injected by the dynamic clamp. This protocol was repeated in four different conditions in the following sequence in Figure 2B: (1) under control conditions; (2) with the dynamic clamp canceling the native I_{NaP}, i.e., an outward current equal in size to the calculated inward I_{NaP} was injected into the cell; (3) with I_{NaP} blocked by adding 1 μM TTX (dynamic clamp off); and (4) with TTX still present and the dynamic clamp turned back on, now with the calculated I_{NaP} injected as an inward current, thereby "restoring" I_{NaP}. In Figure 2C, the voltage responses from Figure 2B are shown superimposed, illustrating that elimination of I_{NaP} by either dynamic clamp ((1) + (2)) or TTX ((1) + (3)) reduced the depolarizing slope beyond ~ -65 mV and reduced spiking. Furthermore, the two methods had virtually identical effects on the subthreshold voltage response ((2) + (3)). The dynamic clamp also fully restored the effect of I_{NaP} after its blockade by TTX, thus reproducing the subthreshold voltage response under control conditions ((1) + (4)).

These data yielded two sets of measurements of I_{NaP} at each subthreshold potential: the TTX-sensitive I_{NaP} and the I_{NaP} that was canceled by the dynamic clamp (the method is illustrated in Figure S1). In addition, we measured I_{NaP} in voltage clamp by applying a voltage ramp from −88 to −38 mV and subtracting the current response before and after adding TTX (n = 8; Figure S2A). These three data sets were all plotted in Figure 2D, showing that the values for I_{NaP} obtained by TTX blockade during current clamp and voltage clamp and by dynamic clamp recording were all virtually identical, thus confirming the validity of our dynamic-clamp approach.

Prediction from Modeling: I_{NaP} Mediates Voltage-Dependent Amplification of AHPs

A noninactivating voltage-gated inward current such as I_{NaP} has two types of effects: (1) a simple, general depolarizing effect and (2) a set of more dynamic effects derived from its voltage dependence and the negative slope resistance that it mediates. In this study, we focused on the latter effects. Therefore, whenever I_{NaP} was changed, in the model or in experiments, we always compensated the change in the background membrane potential by injecting steady depolarizing current, in order to study the voltage-dependent effects of I_{NaP} at comparable membrane potentials.

Thus, when using the model to explore whether I_{NaP} can modulate AHPs (Figure 3), we held the membrane
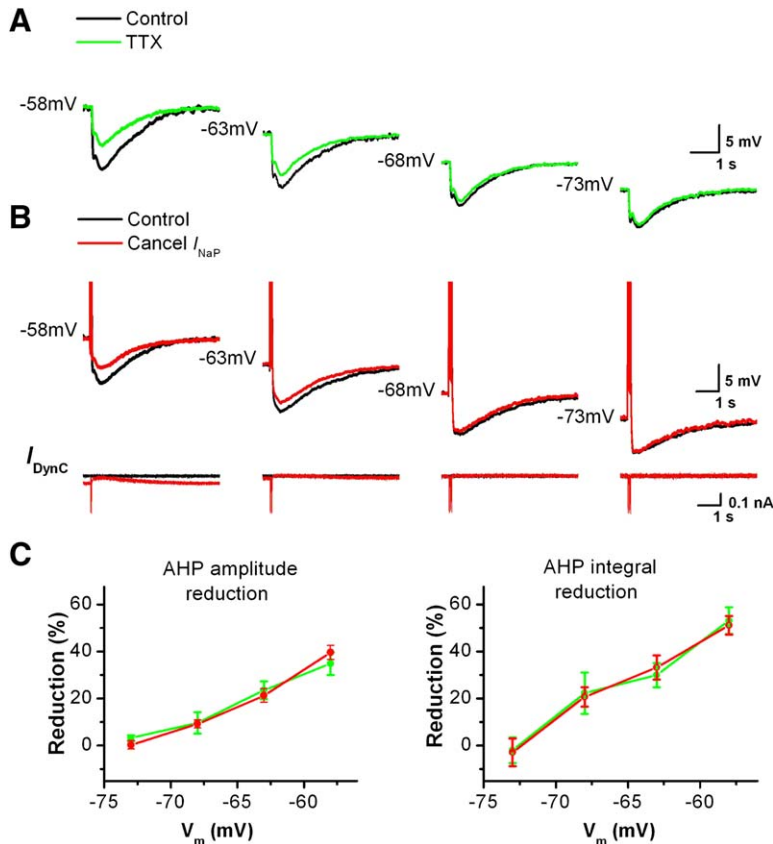
potential at various potentials ranging from −58 to −80 mV by steady-current injection and evoked action potentials followed by AHPs. AHPs are enhanced by depolarization due to increased driving force for K⁺ (Madison and Nicoll, 1984; Storm, 1989). In order to compensate for this effect and compare the impact of I_{NaP} on AHPs of similar amplitudes at different potentials, we evoked more spikes from hyperpolarized holding potentials than at depolarized potentials. When repeating this with and without I_{NaP}, we observed a substantial I_{NaP}-dependent enhancement of the AHPs, and this effect increased with depolarization (Figure 3A, upper traces). The lower traces in Figure 3A show I_{NaP} during this protocol. Figure 3B summarizes the reduction of the AHP peak amplitude (left) and AHP integral (right) as a function of the holding potential. The model also showed a similar voltage-dependent amplification of AHPs following a single spike (Figure S3).

The model was also used to study how AHP amplification by I_{NaP} depends on the AHP amplitude (Figure S4). We found that the amplification was greatest for the AHP following a single spike (Figure S4B).

### Experimental Test: I_{NaP} Mediates Voltage-Dependent Amplification of AHPs

We next used dynamic clamp and TTX to test our theoretical predictions regarding AHP amplification by I_{NaP}. Since TTX also blocks action potentials, we could not use it for testing the effect of I_{NaP} on spike-evoked AHPs. Instead, we injected a current waveform that was designed to evoke a voltage response similar to a spike-evoked AHP (Figure 4A; for details, see Supplemental Data).

For comparison with our model simulations (Figure 3), we tested these artificial "AHPs" at various holding potentials (Figure 4A). In order to obtain roughly constant "AHP" amplitudes (cf. Figure 3A), the amplitude of the current waveform was adjusted by a scaling factor. In all cells tested (n = 5), blockade of I_{NaP} with TTX substantially reduced the "AHPs" in a voltage-dependent manner (Figure 4A), in agreement with our simulations (Figure 3A). Next, we performed an equivalent test with the dynamic clamp, now with real spike-evoked AHPs. Like in the modeling, spikes were evoked by a train of short current pulses at various holding potentials (Figure 4B). Again, to obtain comparable AHP amplitudes, it was necessary to trigger more spikes at hyperpolarized than at depolarized holding potentials. Cancellation of I_{NaP} by dynamic clamp reduced the AHPs in a voltage-dependent manner, in agreement with the model prediction (Figure 3A) and with TTX blockade (Figure 4A). Figure 4C summarizes the reduction in AHP amplitude (left panel) and integral (right) at the various holding potentials. These data confirm our hypothesis that I_{NaP} substantially enhances AHPs in a voltage-dependent manner and that the dynamic clamp is a reliable tool for studying I_{NaP} functions.

Prediction from Modeling: I_{NaP} Changes the Frequency-Current Plots

AHPs provide a negative-feedback control of the spike frequency during repetitive firing. It has previously been
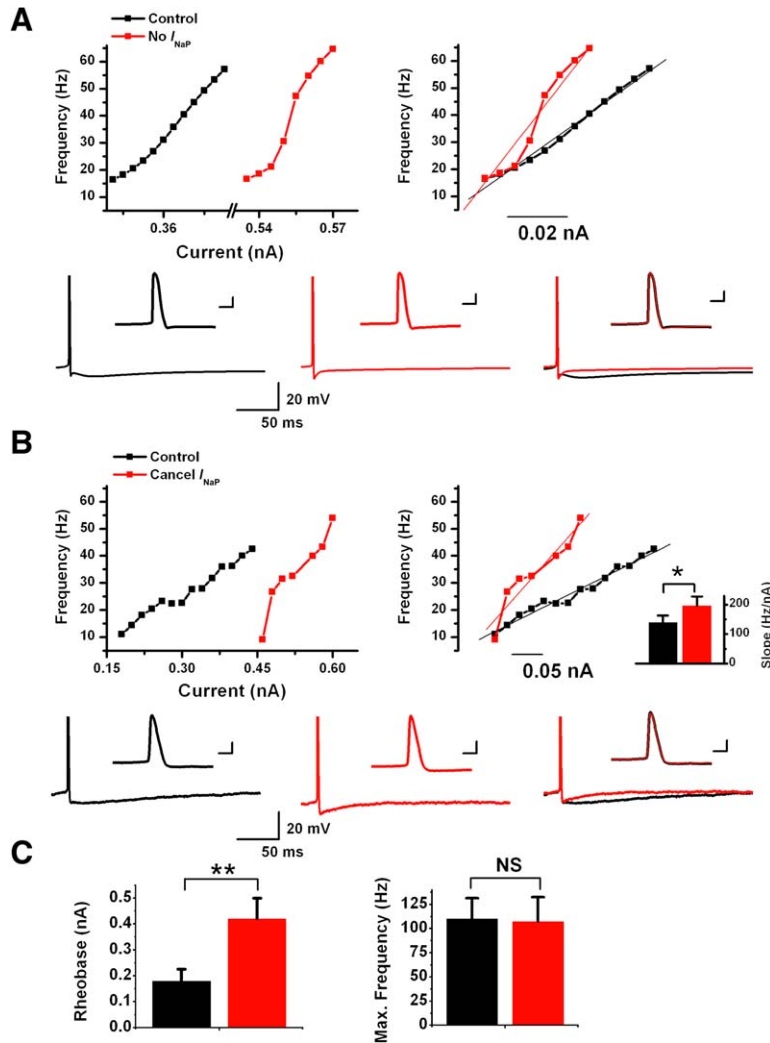
Figure 5. Model Simulations and Electrophysiological Results Showing the Effect of I_{NaP} on Current-to-Spike Frequency Transduction

(A) Frequency-current (f/I) plots with I_{NaP} (black: control) and without I_{NaP} (red) of the average frequency of the first four spikes (range ∼ 15–60 Hz) in response to injection of rectangular current pulses (1 s duration, 5 pA increments). The f/I slope for this range increased by 78% when I_{NaP} was blocked, as shown by the superimposed f/I plots fitted with a linear function (upper right panel). Lower panels show the first action potential and its AHP at rheobase with I_{NaP} (black), without I_{NaP} (red), and superimposed (right). Insets show the spikes at an expanded timescale (scale bars: 2 ms, 20 mV).
(B) Experimental f/I plots obtained from a CA1 pyramidal cell according to the protocol described in (A), before (black) and after (red) canceling I_{NaP} by dynamic clamp. Linear fits of the f/I curves (right panels) showed that canceling I_{NaP} increased the f/I slope, on average by 43% for all cells tested (n = 7, *p = 0.015). Lower panels show the effect of I_{NaP} on the spikes and AHPs (black: control; red: no I_{NaP}; scale bars: 2 ms, 20 mV).
(C) Blocking I_{NaP} significantly increased the rheobase (left panel) (control: 0.18 ± 0.05 nA; I_{NaP} canceled: 0.42 ± 0.08 nA; n = 7, **p < 0.01) while the maximal saturating frequency (1/first ISI) was unchanged by canceling I_{NaP} (right panel) (control: 110 ± 21 Hz; I_{NaP} canceled: 107 ± 25 Hz; n = 3, NS: not significant).

shown that K+ currents underlying AHPs affect the f/I gain (Madison and Nicoll, 1984; Peters et al., 2005; Gu et al., 2005). Since I_{NaP} enhances AHPs (Figures 3 and 4), it might enhance AHP-mediated negative feedback. On the other hand, since I_{NaP} is known to amplify the response to subthreshold depolarizing input, it might also increase the f/I gain. To test whether and how I_{NaP} affects the f/I curves, we performed model simulations.

In the model, rectangular depolarizing-current pulses increasing in steps of 5 pA were injected at the soma. Figure 5A shows the average frequency of the first four spikes (corresponding to a typical spike number in bursts recorded in behaving rats; Harris et al., 2001), plotted as a function of the injected current. Compared to the control situation, blockade of I_{NaP} shifted the f/I curve to the right, increasing the rheobase by 168 pA. This reduced excitability was an expected consequence of the loss of I_{NaP}. In contrast, the slope of the f/I curve was increased by blocking I_{NaP}, as shown by the superimposed f/I curves (Figure 5A, right). The overall slope of the f/I curve, as determined by linear fitting, was increased by 78% by blocking I_{NaP}. In parallel, blockade of I_{NaP} strongly reduced the AHPs, whereas the spike shape was not noticeably affected (Figure 5A, bottom).

The f/I slope for the first interspike interval (ISI) increased by 44% when blocking I_{NaP} (Figure S5A).

Experimental Test: I_{NaP}-Mediated Changes in Frequency-Current Plots

Next, we experimentally tested the predictions regarding the f/I plots. Using the same protocol as in the model, we constructed the f/I curves. For each current step, the cell was tested with and without canceling I_{NaP} by dynamic clamp, in an interleaved sequence, to avoid spurious effect due to changes in input resistance or other factors during recording. Again, the experimental results (Figure 5B) were in good qualitative agreement with the theoretical predictions. Canceling I_{NaP} consistently increased the slope of the f/I plot. For the first four spikes, the average increase was 43% (Figure 5B, right; control: 140 ± 23 Hz/nA; I_{NaP} canceled: 196 ± 32 Hz/nA; p = 0.015, n = 7). For the first ISI, the f/I slope increased by 65% when I_{NaP} was canceled (Figure S5B; control: 160 ± 51 Hz/nA; I_{NaP} canceled: 266 ± 86 Hz/nA; p = 0.03, n = 7). The lower panels of Figure 5B show that elimination of I_{NaP} by dynamic clamp did not affect the spike shape but reduced the AHP, in close agreement with the modeling results (Figure 5A).

A

Control   Cancel I_{NaP}

10 mV
0.2 s

0.5   0.5
0.0   0.0
-0.5   -0.5

0.2 s

B

Control   Cancel I_{NaP} Superimposed

Cumulative Probability
100   100   100
50   50   50
0   0   0
0.0 0.3 0.6   0.0 0.3 0.6   0.0 0.3 0.6
ISI (s)   ISI (s)   ISI (s)

C

Control   Cancel I_{NaP}
Count
100   100   0.5
                          0.4
50   50   0.3
                          0.2
                          0.1
0   0   0.0
0.0 0.3 0.6   0.0 0.3 0.6   control Dyn. Clamp
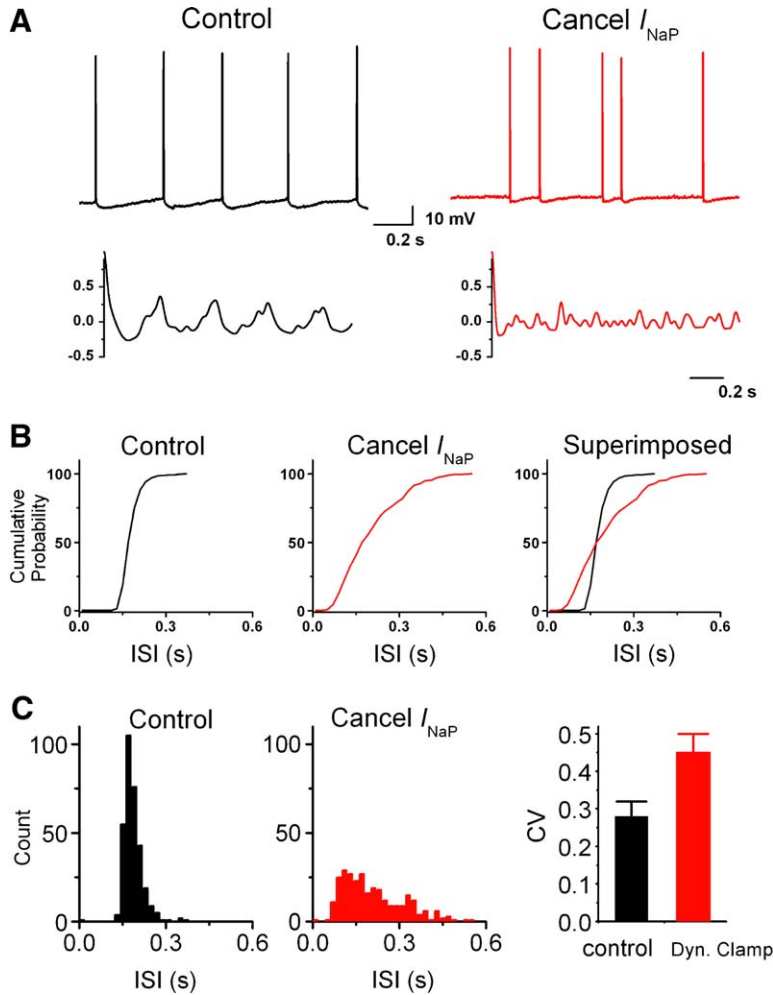ISI (s)   ISI (s)   CV

Figure 6. Electrophysiological Results Demonstrating Disruption of Firing Regularity by Removing I_{NaP}

(A) Typical recording of steady-state (i.e., fully adapted) repetitive firing of a CA1 pyramidal cell in response to a constant depolarizing-current injection under normal conditions (black). After canceling I_{NaP} by dynamic clamp (red), the AHPs were reduced in amplitude and the firing became less regular. The intensity of the injected steady current was adjusted to keep the average firing the same (~3 Hz) in both conditions (control: 3.0 Hz; I_{NaP} canceled: 2.9 Hz). The autocorrelation plots (lower panels, digitally filtered at 15 Hz) indicate that the regularity of firing was reduced when I_{NaP} was canceled (n = 6).
(B) Cumulative-probability plot of the ISIs from data obtained with a protocol similar to that described in (A) for control (black) and with I_{NaP} canceled (red) (n = 6). Data were collected over long periods (5 s–1 min) after the firing frequency had fully adapted.
(C) (Left) Same data as in (B) plotted as histograms. (Right) The CV of ISIs for all cells tested under control conditions (black) and when I_{NaP} was canceled (red) (n = 6; p = 0.02). One hundred micromolar DNQX, one hundred micromolar DL-APV, and ten micromolar free base of bicuculline were present in all experiments.

The experiments and simulations illustrated in Figures 5A and 5B focused on low-frequency firing. We next explored the effect of I_{NaP} on the full dynamic range of firing by injecting depolarizing-current pulses of increasing intensity. In our model, the discharge frequency saturated at a similar frequency (~240 Hz) with and without I_{NaP}. Likewise, in the slice experiments, each cell reached the same maximal discharge frequency with I_{NaP} intact or canceled by dynamic clamp (control: 110 ± 21 Hz; I_{NaP} canceled: 107 ± 25 Hz; n = 3). In contrast, the rheobase was always significantly increased by canceling I_{NaP} (control: 0.18 ± 0.05 nA, I_{NaP} canceled: 0.42 ± 0.08 nA; n = 7, p < 0.01) (Figure 5C).

Experimental Result: I_{NaP}-Mediated AHP Amplification and Increased Regularity of Repetitive Firing

We next studied the effect of I_{NaP} on the regularity of repetitive firing by comparing steady-state firing (Figure 6A) before and after canceling I_{NaP} by dynamic clamp in the same CA1 cell. Cancellation of I_{NaP} strongly reduced the AHPs, as well as the peaks in the autocorrelation plots of spike timing (Figure 6A, bottom), indicating disruption of the spiking periodicity. Similar results were observed in all cells tested in this way (n = 6).

To further examine this effect, we evoked low-frequency, steady repetitive firing (~3 Hz) by injecting depolarizing current and compared the ISI distributions plotted as cumulative probability (Figure 6B) and histograms (Figure 6C). Canceling I_{NaP} increased the ISI variability, as indicated by a significant increase in the coefficient of variation (CV = SD/mean; Figure 6C; control: 0.28 ± 0.04; I_{NaP} canceled: 0.45 ± 0.05; p = 0.02, n = 6). Interestingly, when I_{NaP} was canceled, we noticed an increase in the firing threshold and a decrease in both spike amplitude and rate of rise during steady-state repetitive firing (Table 1), suggesting reduced recovery of the spike-generating Na current, I_{NaT}, due to

Table 1. Action Potential Parameters during Steady-State Firing from Electrophysiological Recordings

	Action Potential Threshold (mV)	Action Potential Rate of Rise (mV/ms)	Action Potential Amplitude (mV)
Control	−55.2 ± 1.4	190.4 ± 14.6	81.6 ± 2.12
I_{NaP} blocked	−52.3 ± 1.6	152.3 ± 6.4	76.6 ± 2.28
p value	0.003	0.033	0.012

Action potentials were randomly selected under normal conditions (control) and when I_{NaP} was blocked by dynamic clamp (n = 4).
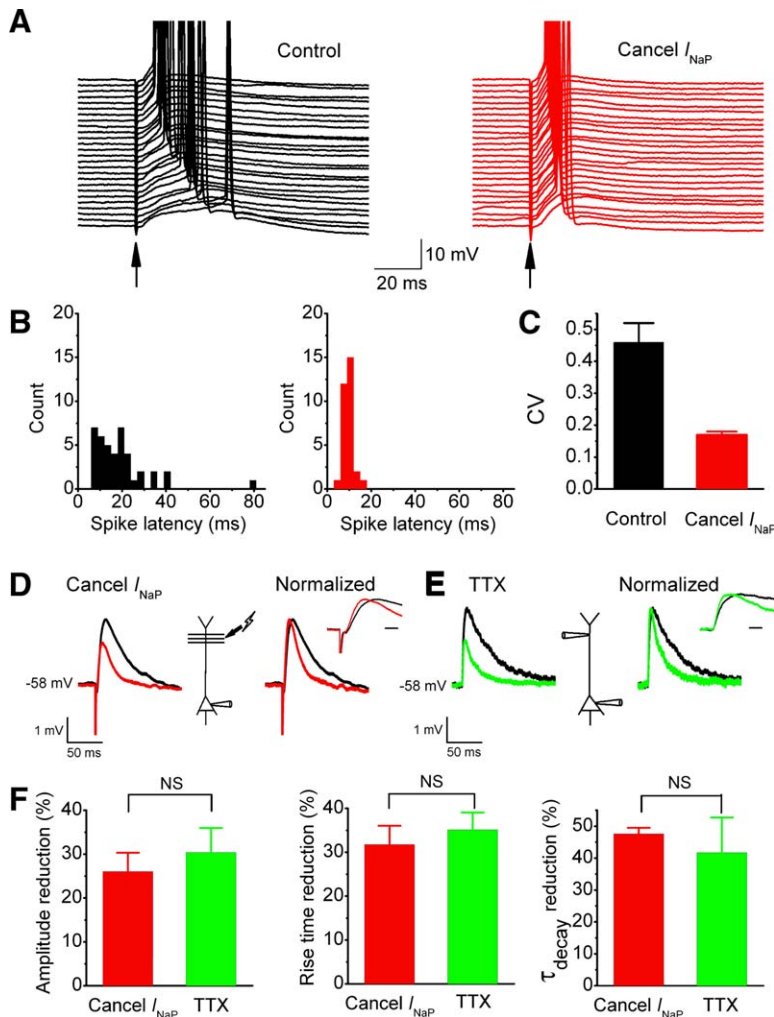
Figure 7. Electrophysiological Results Demonstrating that I_{NaP} Reduces the Precision of Spike Timing Evoked by Single EPSPs

(A) Somatic EPSPs were evoked by stimulation of axons in the middle of stratum radiatum at 0.2–0.3 Hz. The EPSPs triggered a spike with a probability of 0.48 ± 0.06 (holding V_m −58 mV). When I_{NaP} was canceled by dynamic clamp, stimulation strength was increased to evoke spikes with a probability (0.41 ± 0.04, n = 8, p > 0.05) similar to before.
(B) Distributions of spike time delay measured from the onset of the EPSP to the spike under normal conditions (left, n = 41 trials) and when I_{NaP} was canceled (right, n = 31 trials).
(C) CV of spike time delay (control: 0.46 ± 0.06; I_{NaP} canceled: 0.17 ± 0.01; n = 8, p < 0.01).
(D and E) Effect of canceling I_{NaP} by dynamic clamp (n = 5) or 1 μM TTX (n = 5), respectively, on somatic EPSP parameters (average of 20–30 sweeps).
(D) Subthreshold EPSPs were evoked by stimulating axons in stratum radiatum (100 μM APV was added).
(E) A simulated EPSP current waveform was injected through a whole-cell patch pipette positioned ∼220 μm from the soma on the apical dendrite.
(F) Somatic dynamic clamp and bath application of TTX showed a similar reduction in EPSP amplitude (dynamic clamp: 26% ± 4.3%; TTX: 30% ± 5.5%), rise-time (dynamic clamp: 31% ± 4.3%; TTX: 37% ± 4.1%), and decay-time constant (dynamic clamp: 47% ± 1.9%; TTX: 42% ± 11%). NS: p > 0.05; inset scale bars in (D) and (E): 5 ms. Ten micromolar free base of bicuculline was present in all experiments.

AHP reduction. In accordance with this interpretation, a few neurons could not sustain high-frequency steady firing when I_{NaP} was canceled. Canceling I_{NaP} also increased the ISI variability during short-lasting nonadapted spike trains (∼6 Hz) evoked by depolarizing square pulses (data not shown).

Since our model is by nature deterministic, and therefore can only produce perfectly repeatable repetitive firing in response to steady depolarizing current (Koch, 1999), the increased ISI variability observed by blocking I_{NaP} was not reproduced by our model.

Experimental Result: I_{NaP} Reduces the Precision of Spike Timing Evoked by Near-Threshold EPSPs

In contrast to rhythmic firing evoked by sustained depolarization, where I_{NaP} makes the firing more regular and predictable, Fricker and Miles (2000) suggested that I_{NaP} reduces spike precision in response to near-threshold EPSPs. However, the lack of specific I_{NaP} blockers has so far prevented direct testing of this idea.

To analyze EPSP-spike coupling experimentally, we held CA1 cells at −58 mV and evoked EPSPs by stimulating axons in stratum radiatum, adjusting the stimulus so that the EPSPs triggered spikes with ∼50% probability (Figure 7A, left). The action potentials often arose from plateau potentials with a highly variable delay

(∼5–80 ms). In contrast, when dynamic clamp was used to cancel I_{NaP} (while maintaining ∼50% spiking probability by stimulus adjustment), the spike time variability was significantly reduced (Figure 7A, right). This is also shown by the spike latency distribution (Figure 7B). Blocking I_{NaP} reduced the CV of spike latency by 57.2% ± 4.9% (Figure 7C; n = 8, p < 0.01).

Figure 7D shows a typical example of how cancellation of I_{NaP} by dynamic clamp reduced the amplitude, rise time (see inset), and decay time of subthreshold EPSPs. To compare the effects of dynamic clamp versus TTX, we performed dual dendritic and somatic whole-cell recordings (Figure 7E; n = 5). The apical trunk was patched 180–320 μm (mean: 220 ± 33 μm) from the soma. An EPSP-like current waveform was injected into the dendrites to evoke an artificial somatic "EPSP" with amplitude, rise, and decay kinetics similar to the synaptically evoked EPSPs (Figure 7E; see also Supplemental Data). Bath application of TTX reduced the somatic EPSP (Figure 7E) in the same way as by dynamic clamp (Figure 7D). Thus, there was no significant difference between the effects of TTX and dynamic clamp on EPSP amplitude, rise-time, or decay-time constant (Figure 7F). These similarities indicate that our dynamic clamp approach is valid and suggest that the amplifying effect is largely due to a perisomatic I_{NaP}.
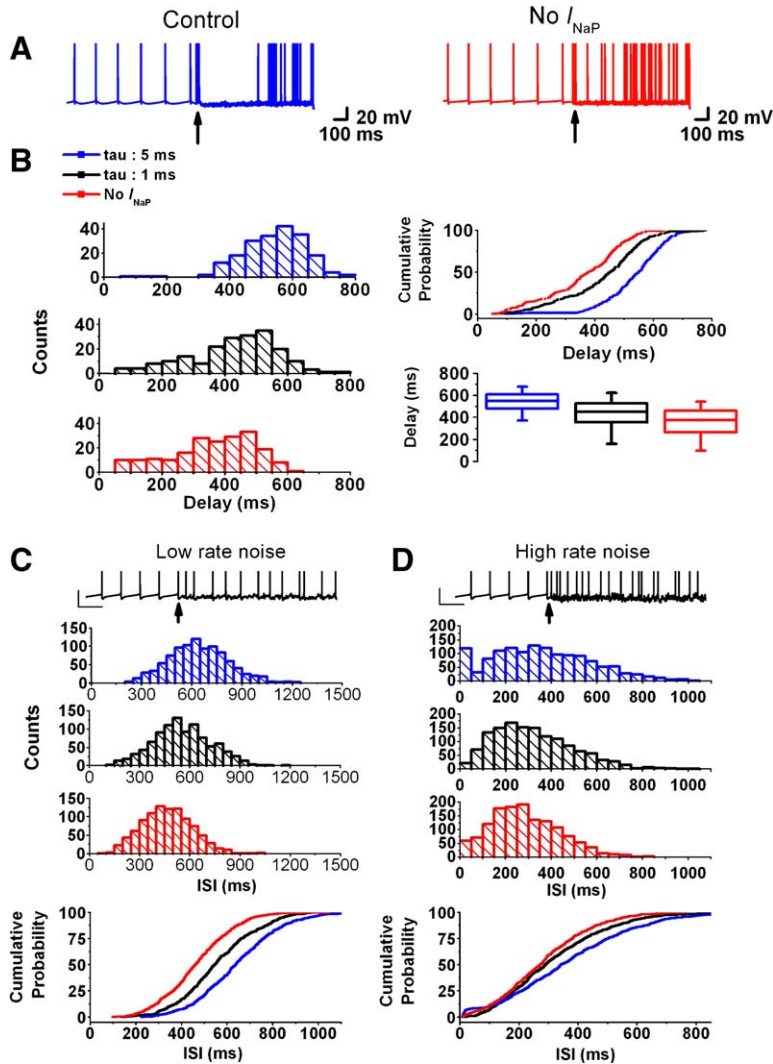
Figure 8. Model Simulations Showing that I_{NaP} Affects Spike Delay and ISI Variability in the Presence of Synaptic Noise

(A) Following steady-state repetitive firing in response to a constant depolarizing current, a train of brief current pulses (11 pulses at 100 Hz, each 1 ms, 1 nA) was injected (at ↑) in the model. Each pulse evoked an action potential. At the end of the pulse train, synaptic noise was injected, consisting of a sum of independent Poisson EPSCs (0.7 ms^{-1}) and IPSCs (0.3 ms^{-1}). Responses were obtained under normal conditions (left) and with no I_{NaP} in the model (right); 10 sample traces for each case are shown superimposed. I_{NaP} had an activation time constant of 5 ms.

(B) Results from multiple simulations of the kind shown in (A). (Left) Histograms of firing delays following the pulse train under three different conditions (200 simulations for each condition): $\tau_{a,NaP}$ = 5 ms (blue), $\tau_{a,NaP}$ = 1 ms (black), and no I_{NaP} (red). (Right) Cumulative-probability plots (top) and box plots (bottom) of the same data as shown in the histograms.

(C) Histograms showing the distribution of ISIs during repetitive firing evoked by rectangular depolarizing-current pulses (20 s duration) combined with synaptic noise. Once steady-state firing was achieved (~1.2 Hz), synaptic noise (as described for [A]; EPSCs: 0.07 ms^{-1}, IPSCs: 0.03 ms^{-1}) was introduced (at ↑). The three histograms and cumulative probability plots show the ISI distributions for the different conditions.

(D) Same protocol as in (C) but in the presence of synaptic noise at a higher rate (EPSCs: 0.7 ms^{-1}; IPSCs: 0.3 ms^{-1}). Scale bars in (C) and (D): 1 s and 20 mV.

In order to test whether the results shown in Figures 7A–7C depended on stochastic transmitter release or transmitter receptors, we also did dual-patch experiments similar to that shown in Figure 7E, but after blocking both excitatory synapses (with 1 mM kynurenic acid or 10 μM DNQX plus 100 μM DL-APV) and inhibitory synapses (100 μM picrotoxin or 10 μM free base of bicuculline). We then mimicked the protocol used in Figures 7A–7C by injecting artificial "EPSCs" in the dendrite (184 ± 13 μm from the soma). When I_{NaP} was canceled by dynamic clamp, the CV of the somatic spike latency was reduced by 48.1% ± 5.5% (n = 5, p = 0.01) (spike probability; control: 54% ± 6%; I_{NaP} canceled: 46% ± 5%; p = 0.33). This result indicates that the I_{NaP}-induced reduction in spike time precision is not dependent on stochastic transmitter release or receptors, although we cannot exclude that these may contribute under normal conditions.

Prediction from Modeling: I_{NaP} Affects Spike Delay and ISI Variability in the Presence of Synaptic Noise

The disruption of firing regularity by blocking I_{NaP} (Figure 6A) and the I_{NaP}-dependent variable spike timing in response to EPSPs (Figure 7A) presumably reflect intrinsic stochastic processes, possibly ion-channel gating, since both phenomena were seen during synaptic blockade (Figures 6 and 7). However, for a neuron embedded in an active network in vivo, background synaptic activity is often a far more important source of noise (Destexhe et al., 2003). To begin analyzing the effects of I_{NaP} on refractoriness and spiking regularity under such conditions, we performed simulations with Poisson-distributed background synaptic noise.

Long-lasting depolarizing-current pulses were injected in the model soma to evoke repetitive firing (~5 Hz; Figure 8A). During steady-state firing, a high-frequency spike burst was triggered by brief current pulses. The burst evoked a composite AHP (i.e., mAHP and sAHP) that delayed the subsequent discharge. To test the interaction between I_{NaP}, AHPs, and synaptic noise, simulated Poisson-distributed synaptic noise (Chance et al., 2002) was introduced throughout the AHP and subsequent firing, starting at the end of the spike burst (arrow). Elimination of I_{NaP} clearly increased the probability that spikes occurred during the burst-evoked AHP (Figure 8A, right). The average steady firing rate was kept close to ~5 Hz by adjusting the intensity of the long depolarizing-current pulse.

Thus, it appeared that in our model, the amplification of AHPs by I_{NaP} dominated over another likely effect of I_{NaP}: amplification of synaptic noise. However, the relative impact of these two effects is likely to depend on the kinetics of I_{NaP}. Thus, if I_{NaP} activates and deactivates slowly, it may be inefficient in amplifying fast peaks of noise but may still effectively amplify AHPs, thus causing a net increase in AHP-induced spike delay. In contrast, if I_{NaP} activation is rapid, amplification of fast synaptic potentials may tend to cancel the AHP amplification effect, thus reducing the firing delay.

In order to test these hypotheses, we performed several series of simulations similar to those illustrated in Figure 8A but with different values for the activation-time constant of I_{NaP} ($\tau_{a,NaP}$). Figure 8B shows the distribution of the delays in three different conditions: (1) $\tau_{a,NaP}$ = 5 ms, (2) $\tau_{a,NaP}$ = 1 ms, and (3) I_{NaP} "blocked." The resulting delay distributions (plotted as histograms and cumulative-probability and box plots; Figure 8B) show that I_{NaP} strongly increased the AHP-induced spiking delay when I_{NaP} was relatively slow ($\tau_{a,NaP}$ = 5 ms; Figures 8A and 8B), but this effect was reduced when I_{NaP} was faster ($\tau_{a,NaP}$ = 1 ms). The CV of the compound AHP-induced spike delay was 0.19 for $\tau_{a,NaP}$ = 5 ms, 0.29 for $\tau_{a,NaP}$ = 1 ms, and 0.37 without I_{NaP}. This indicates that I_{NaP} reduced the variability of the spike delay in the presence of synaptic noise.

Next, we explored how the amplification of AHPs affected the firing regularity during ongoing synaptic activity (Figures 8C and 8D). In the model, a square depolarizing-current pulse was injected into the soma to evoke repetitive firing. Once steady-state firing was achieved, random synaptic activity (like in Figures 8A and 8B) was introduced (arrows in Figures 8C and 8D, top panels), and the resulting ISI distributions were plotted (Figures 8C and 8D). We performed simulations for two different rates of noise (10 times higher Poisson rate in Figure 8D than in Figure 8C), and for each rate, we tested three variants of I_{NaP}: (1) $\tau_{a,NaP}$ = 5 ms, (2) $\tau_{a,NaP}$ = 1 ms, and (3) I_{NaP} "blocked." In each case, the average steady firing rate before the introduction of synaptic activity was kept similar by adjusting the long pulse amplitude. Blockade of I_{NaP} shifted the ISI distribution to higher frequencies, indicating a reduced refractoriness, whereas slowing the kinetics of I_{NaP} shifted the ISI distribution toward lower frequencies, indicating increased refractoriness, as also shown by cumulative-probability plots (bottom panels). The latter result agrees with those shown in Figure 8B. For the lowest synaptic noise rate (Figure 8C), the CV was 0.26 for $\tau_{a,NaP}$ = 5 ms, 0.29 for $\tau_{a,NaP}$ = 1 ms, and 0.33 without I_{NaP}, thus indicating that I_{NaP} reduced the ISI variability. For the highest synaptic noise rate (Figure 8D), the CV was 0.45 for $\tau_{a,NaP}$ = 1 ms and 0.56 without I_{NaP}.

Overall, these results were qualitatively similar for the two rates of synaptic noise; in both cases, the fast I_{NaP} reduced the ISI variability. However, for high noise and $\tau_{a,NaP}$ = 5 ms, the CV was 0.60, i.e., higher than without I_{NaP}. This deviation was due to a more frequent occurrence of brief ISIs (<50 ms) for $\tau_{a,NaP}$ = 5 ms (top histogram in Figure 8D). Examination of the simulated spike trains showed that this particular effect was caused by I_{NaP}-dependent enhancement of an afterdepolarization following each spike.

Discussion

This study revealed that I_{NaP} in CA1 pyramidal cells has seemingly contrasting or "opposite" effects on two different aspects of neuronal input-output relations: (1) two different indexes of excitability (rheobase and f/I gain) and (2) two different indexes of spike timing variability (regularity of repetitive firing and spike time precision during transient synaptic excitation).

By computational modeling, we arrived at the robust prediction that I_{NaP} amplifies the AHPs and reduces the f/I gain in parallel with a reduction in rheobase. These predictions were all confirmed by patch-clamp experiments using dynamic clamp and/or channel blockade by TTX. To our knowledge, this is the first demonstration that an inward, depolarizing current can reduce the f/I gain and enhance the hyperpolarizing effect of spike-triggered outward K$^+$ currents (without increasing the K$^+$ current itself).

Furthermore, our experiments showed that I_{NaP} increased spike regularity during repetitive firing in response to sustained depolarization, although it decreased spike timing precision in response to single EPSPs. These results demonstrate for the first time seemingly opposite roles of I_{NaP} in regulating two forms of spike time variability. We suggest that a dynamic interaction between I_{NaP} and neuronal stochastic processes ("noise") causes these effects (see below).

Finally, model simulations demonstrated an I_{NaP}-mediated increase in the relative refractory period and decrease in ISI variability under conditions resembling an active network in vivo. This novel result leads to the prediction that I_{NaP} may enhance refractoriness and discharge regularity in pyramidal cells in the intact brain during behavior. Future experiments will be needed to test these predictions.

Mechanism of AHP Amplification

It may seem surprising that I_{NaP}, being an inward, depolarizing current, can amplify hyperpolarizing potentials such as AHPs. Nevertheless, it has been shown that tonically active inward currents like I_{NaP} or a Ca^{2+} window current can amplify inhibitory postsynaptic potentials (IPSPs) in neocortical (Stuart, 1999) and thalamocortical neurons (Williams et al., 1997), respectively. In a recent study, we found that I_{NaP} enhances the hyperpolarizing as well as the depolarizing phase of the oscillatory response at theta frequencies in hippocampal pyramidal neurons (Hu et al., 2002).

In all these cases—AHPs, IPSPs, and theta oscillations—the ability of I_{NaP} to amplify hyperpolarizing potentials follows from the negative slope conductance introduced by I_{NaP} (Crill, 1996) and can be explained as follows. At depolarized potentials, I_{NaP} is tonically active, causing a sustained depolarization of the cell. When a hyperpolarizing event such as an AHP occurs, I_{NaP} is partly or fully turned off by the hyperpolarization. The resulting loss in inward Na$^+$ current, which is equivalent to an increase in outward current, causes an increased hyperpolarization, i.e., an amplification of the AHP. Neither the molecular identity nor the location of the channels mediating I_{NaP} is known with certainty. I_{NaP} may result from fast-inactivating Na$^+$ channels that have switched into a noninactivating mode

(Alzheimer et al., 1993; Crill, 1996). Both soma and dendrites contain fast-inactivating Na⁺ channels, but the highest density is thought to be in the axon, including its initial segment (French et al., 1990; Stuart and Sakmann, 1995). Such a location would make I_{NaP} highly suitable for amplifying AHPs and for affecting firing behavior, especially since available evidence suggests that K⁺ channels underlying the mAHP (Kv7/KCNQ/M-type K⁺ channels) and sAHP are also located perisomatically (Sah and Bekkers, 1996; Devaux et al., 2004), thereby favoring an efficient interaction.

We propose that it is not a coincidence that I_{NaP} has a range of activation covering the voltage ranges of AHPs and spike triggering and that it is strongly voltage dependent. Rather, these specific properties may serve its main function, i.e., its "evolutionary raison d'etre." Thus, it seems plausible that I_{NaP} is tuned to interact with AHPs and action potential generation. Therefore, we chose in this study to focus mainly on the dynamic, voltage-dependent effects of I_{NaP} rather than its general depolarizing effects, which could be performed even by a simple leak current.

Why Does I_{NaP} Reduce the f/I Gain?

One might expect that I_{NaP}, which is known to enhance the effect of every depolarizing input within its activation range, would increase the f/I slope. Why did we find the exact opposite result? It is unlikely that the conductance caused by the open NaP channels (g_{NaP}) contributes appreciably to shunting of the injected current since g_{NaP} is only a small fraction of the total K⁺ conductance (g_K) during the ISIs. The I_{NaP}-induced enhancement of AHPs may be a more likely cause since AHPs exert negative-feedback regulation of the discharge frequency. However, this factor alone does not explain why I_{NaP} should increase the impact of AHPs more than that of the depolarizing injected current. Instead, we propose that the amplification of depolarizing current by I_{NaP}, which depends on a positive feedback between depolarization and I_{NaP} activation, will be largely disabled during repetitive firing because AHPs maintain the membrane potential between spikes at a negative level. Thus, I_{NaP} will be nearly constant for all values of injected current and will therefore cause primarily a leftward shift of the f/I curve, thus leaving other effects of I_{NaP} to influence the f/I slope. So, I_{NaP} appears to exert two opposing effects on excitability: (1) In the voltage range negative to the spike threshold, it increases excitability in an additive manner by providing an extra depolarizing inward current, thus lowering the rheobase; and (2) on the other hand, for suprathreshold stimuli, I_{NaP} appears to weaken excitability in a multiplicative manner (Chance et al., 2002) by reducing the f/I slope.

How Does I_{NaP} Increase Regularity of Repetitive Firing?

Elimination of I_{NaP} by dynamic clamp increased the variability of ISIs. This indicates that I_{NaP} serves to increase the regularity of repetitive firing. However, this experimentally observed effect (Figure 6) was not seen with our deterministic model (data not shown), suggesting that it depends critically on stochastic events, i.e., noise. We propose that two mechanisms may underlie the I_{NaP}-induced increase in regularity.

(1) First, by amplifying AHPs, I_{NaP} increases the relative refractoriness that suppresses noise-triggered irregular discharge (de Ruyter van Steveninck et al., 1997). This hypothesis is supported by the finding that a similar effect was produced when simulated synaptic noise was incorporated in our model (Figure 8). However, it should be stressed that the situation shown in Figure 8 was quite different from the repetitive firing shown in Figure 6, when the noise level was far lower. Additional simulations with lower noise levels, comparable to the baseline noise in our recordings, were insufficient to reproduce the experimental effect seen in Figure 6 (data not shown). This strongly suggests that the increase in refractoriness caused by AHP amplification alone is insufficient to explain how I_{NaP} increases the regularity of repetitive firing. Therefore, we suggest that the following mechanism also contributes.

(2) It is known that stochastic gating of ion channels may cause irregular repetitive firing when there are few available spike-generating channels (Skaugen and Walloe, 1979; Schneidman et al., 1998). This may occur when the AHPs are shallow after elimination of I_{NaP}, thus reducing deinactivation of I_{NaT} during the ISIs. The remaining active I_{NaT} channels may be so few that channel noise becomes important for spike initiation. Conversely, when I_{NaP} amplifies the AHPs, the more numerous deinactivated Na⁺ channels reduce spike jitter. This hypothesis is supported by the results of Gasparini and Magee (2002), who found that the I_{NaT} inactivation curve is very steep (slope factor ~ 7), with a midpoint within the voltage range traversed by AHPs ($V_{0.5}$ ~ −66 mV). Since recovery from inactivation is relatively slow (~100 ms) in this voltage range (Sah et al., 1988), it is likely that I_{NaP}-dependent amplification of AHPs is important for deinactivation of I_{NaT} between spikes. This hypothesis was further supported by simulations indicating that I_{NaT} can recover substantially from inactivation during an ISI with a normal AHP (data not shown) and our experimental data showing significant changes in spike threshold, amplitude, and rate of rise (Table 1). The latter data indicate that I_{NaT} recovered more during the I_{NaP}-enhanced AHPs than when I_{NaP} was blocked. Moreover, we found that some of the neurons could not sustain high-frequency firing when I_{NaP} was canceled, probably because of Na⁺ channel inactivation.

Others have shown that partial block of the AHPs by apamin increased the ISI variability in subthalamic neurons (Hallworth et al., 2003), midbrain neurons (Wolfart et al., 2001), and neostriatal neurons (Bennett et al., 2000). Also, blockade of Kv3-mediated AHPs in interneurons resulted in a cumulative Na⁺ channel inactivation (Erisir et al., 1999; Lien and Jonas, 2003). Thus, although the mechanisms of AHP reduction in these cases were profoundly different from I_{NaP} blockade, some of the functional consequences appear to be similar.

How Does I_{NaP} Reduce Spike Time Precision?

The importance of I_{NaP} for spike timing was further illustrated by the observation that I_{NaP} increased the spike time variability in response to evoked EPSPs (Figure 7). Figures 7A–7C show that I_{NaP} amplifies and prolongs near-threshold EPSPs, thus promoting a high spike time variability. This is an interesting contrast to the effect that I_{NaP} makes repetitive firing more regular and

predictable (Figure 6). Again, the effect of I_{NaP} on spike time variability probably reflects its interaction with stochastic events.

Since the effect on spike time precision was also observed in response to injection of artificial EPSP waveforms during blockade of excitatory and inhibitory synaptic transmission, the effect must be independent of stochastic transmitter release. Rather, it may reflect stochastic ion-channel gating due to the relatively small number of channels that are opened near threshold (Schneidman et al., 1998). We suggest that the I_{NaP}-dependent prolongation of near-threshold EPSPs extends the time spent near threshold, thereby increasing the impact of noise on spike timing (Fricker and Miles, 2000).

Physiological Implications of the AHP Amplification
Because AHPs and I_{NaP} coexist in numerous neuronal types (Crill, 1996; Vogalis et al., 2003), their interaction as described in this study is likely to be widespread and may occur in several brain regions.

The information output of neurons is largely defined by the temporal pattern of their spikes. Therefore, it is essential to understand how each neuron transforms its input into a series of spikes. When neurons use a firing-rate code, refractoriness may reduce the dynamic range of neural output by promoting saturation of the firing rate. However, if the information lies in the number or timing of spikes fired during a discrete firing event, then the maximum firing rate may not be the main limiting factor. Because the refractoriness can improve the temporal precision of subsequent spikes in an event, it may lead to a spike count or spike timing of higher fidelity (de Ruyter van Steveninck et al., 1997; Berry and Meister, 1998). When the information output of a neuron is determined by spike timing and coincidence detection (Markram et al., 1997), I_{NaP} is likely to play a significant role in the timing-dependent coding and in synaptic plasticity. Furthermore, I_{NaP} is itself regulated by various modulatory pathways (Cantrell and Catterall, 2001), which may regulate the I_{NaP}-mediated effects reported here.

Amplification of AHPs by I_{NaP} could also be critical for firing regularity in tonic firing neurons (Bennett et al., 2000; Wolfart et al., 2001; Hallworth et al., 2003; Hoebeek et al., 2005) in which disruption of firing regularity has been related to dysfunctional behavior. Indeed, recovery from Na$^+$ channel inactivation between spikes is essential for spontaneously firing neurons (Hausser et al., 2004), both to maintain firing for long periods and to ensure regularity.

In conclusion, by using a computational model that is sufficiently complete to predict spiking properties of hippocampal pyramidal neurons and by using dynamic clamp to tease apart the functional roles of currents that cannot be separated pharmacologically, this study has revealed roles of I_{NaP} in determining neuronal refractoriness, current-to-frequency transduction, firing regularity, and spike timing precision under noisy conditions.

Experimental Procedures

Slice Preparation, Recording, and Analysis
The methods are described in detail in the Supplemental Data. Briefly, whole-cell recordings were obtained from CA1 hippocampal pyramidal cells under visual guidance. During recording, slices were submerged in saline containing (in mM) 125 NaCl, 25 NaHCO$_3$, 1.25 KCl, 1.25 KH$_2$PO$_4$, 1 MgCl$_2$, 2 CaCl$_2$, and 25 glucose and saturated with 95% O$_2$/5% CO$_2$ at 30ºC–35ºC (<0.5ºC variation within each recording). The patch pipettes were filled with a solution containing (in mM) 140 K-gluconate or KMeSO$_4$, 10 HEPES, 2 ATP, 0.4 GTP, 2 MgCl$_2$, and 10 phosphocreatine (resistance: 2–5 MΩ for somatic recording and 8–12 MΩ for dendritic recording). Two Dagan BVC 700A amplifiers (Minneapolis) and Axopatch 1D (Molecular Devices) were used for current-clamp and voltage-clamp recording, respectively. The data were acquired using pCLAMP 9.0 (sampled at 20 kHz) and were analyzed and plotted with pCLAMP 9.0 and Origin 7.0 (Microcal). Pooled data are expressed as mean ± SE, and statistical differences were evaluated by a two-tailed Student's t test (significance level 0.05).

Dynamic Clamp
A dynamic-clamp system (DynClamp2; Pinto et al., 2001) was used to inject an artificial I_{NaP} into the neuron. This system has an update rate of $\sim$10 kHz ($\triangle t \sim 100$ μs) and was run on a Pentium IV computer with a Digidata 1200 as ADC-DAC board (Molecular Devices). The dynamic-clamp software calculates the injected artificial I_{NaP} by a Hodgkin-Huxley equation: $I_{NaP} = G_{max} \times m \times (V_m - E_{rev})$, with dm/dt = $(m \infty - m)/\tau_m$ and $m \infty = 1/(1 + \exp[(V_m - V_{1/2})/V_{slope}])$ and G_{max} = 4.8 nS, E_{rev} = 30 mV, $V_{1/2}$ = −51 mV, and V_{slope} = −4.5 mV. Further details are given in the Supplemental Data.

Computational Methods
In the Supplemental Data, we describe and motivate the CA1 pyramidal-cell model in detail. Briefly, simulations were performed with the Surf-Hippo simulator (Graham, 2004). The cell was represented as a ball-and-stick type of model with five compartments: an isopotential soma (diameter 20 μm) and a dendritic cable (total length 800 μm and diameter 5 μm) consisting of four segments of equal length. This model combines intracellular Ca^{2+} dynamics with 11 active currents, including persistent and transient Na$^+$ currents (I_{NaP} and I_{NaT}) (Borg-Graham, 1999); four voltage-gated K$^+$ currents, I_A, I_D, I_{DR}, and I_M; a fast-inactivating Ca^{2+}- and voltage-dependent K$^+$ current, I_{BK} (Shao et al., 1999); two voltage-gated Ca^{2+} currents, I_{CaN} and I_{CaL}; a hyperpolarization-activated nonspecific cation current, I_h; and a Ca^{2+}-activated sAHP current (I_{sAHP}) (Borg-Graham, 1999). For Figure 8, the excitatory and inhibitory synaptic currents were calculated as $I_{syn} = g_{syn} (E_{rev} - V_m)$. E_{rev} was 0 mV (excitatory) and −80 mV (inhibitory). Presynaptic spike trains were generated by Poisson processes at specific rates. The unitary synaptic conductance was calculated as a difference of exponentials with time constants of 0.1 ms for the rising phase and either 5 ms (excitatory) or 10 ms (inhibitory) for the falling phase (Chance et al., 2002). The peak unitary synaptic conductances were set to 2% (excitatory) or 6% (inhibitory) of the measured resting membrane conductance (Chance et al., 2002).

Supplemental Data
Supplemental Data include five figures, two tables, Supplemental Experimental Procedures, and Supplemental References and can be found with this article online at http://www.neuron.org/cgi/content/full/49/2/257/DC1/.

References

Alzheimer, C., Schwindt, P.C., and Crill, W.E. (1993). Modal gating of Na+ channels as a mechanism of persistent Na+ current in pyramidal neurons from rat and cat sensorimotor cortex. J. Neurosci. *13*, 660–673.

Andreasen, M., and Lambert, J.D.C. (1999). Somatic amplification of distally generated subthreshold EPSPs in rat hippocampal pyramidal neurones. J. Physiol. *519*, 85–100.

Bennett, B.D., Callaway, J.C., and Wilson, C.J. (2000). Intrinsic membrane properties underlying spontaneous tonic firing in neostriatal cholinergic interneurons. J. Neurosci. *20*, 8493–8503.

Berry, M.J., and Meister, M. (1998). Refractoriness and neural precision. J. Neurosci. *18*, 2200–2211.

Borg-Graham, L. (1999). Interpretations of data and mechanisms for hippocampal pyramidal cell models. In Cerebral Cortex, Volume 12: Cortical Models, E.G. Jones, P.S. Ulinski, and A. Peter, eds. (New York: Plenum Press).

Cantrell, A.R., and Catterall, W.A. (2001). Neuromodulation of Na+ channels: an unexpected form of cellular plasticity. Nat. Rev. Neurosci. *2*, 397–407.

Chance, F.S., Abbott, L.F., and Reyes, A.D. (2002). Gain modulation from background synaptic input. Neuron *35*, 773–782.

Crill, W.E. (1996). Persistent sodium current in mammalian central neurons. Annu. Rev. Physiol. *58*, 349–362.

de Ruyter van Steveninck, R., Lewen, G.D., Strong, S.P., Koberle, R., and Bialek, W. (1997). Reproducibility and variability in neural spike trains. Science *275*, 1805–1808.

Destexhe, A., Rudolph, M., and Pare, D. (2003). The high-conductance state of neocortical neurons in vivo. Nat. Rev. Neurosci. *4*, 739–751.

Devaux, J.J., Kleopa, K.A., Cooper, E.C., and Scherer, S.S. (2004). KCNQ2 is a nodal K+ channel. J. Neurosci. *24*, 1236–1244.

Erisir, A., Lau, D., Rudy, B., and Leonard, C.S. (1999). Function of specific K(+) channels in sustained high-frequency firing of fast-spiking neocortical interneurons. J. Neurophysiol. *82*, 2476–2489.

French, C.R., and Gage, P.W. (1985). A threshold sodium current in pyramidal cells in rat hippocampus. Neurosci. Lett. *56*, 289–293.

French, C.R., Sah, P., Buckett, K.J., and Gage, P.W. (1990). A voltage-dependent persistent sodium current in mammalian hippocampal neurons. J. Gen. Physiol. *95*, 1139–1157.

Fricker, D., and Miles, R. (2000). EPSP amplification and the precision of spike timing in hippocampal neurons. Neuron *28*, 559–569.

Gasparini, S., and Magee, J.C. (2002). Phosphorylation-dependent differences in the activation properties of distal and proximal dendritic Na+ channels in rat CA1 hippocampal neurons. J. Physiol. *541*, 665–672.

Graham, L.J. (2004). The Surf-Hippo Neuron Simulation System, version 3.5a (computer program).

Gu, N., Vervaeke, K., Hu, H., and Storm, J.F. (2005). Kv7/KCNQ/M and HCN/h, but not KCa2/SK channels, contribute to the somatic medium after-hyperpolarization and excitability control in CA1 hippocampal pyramidal cells. J. Physiol. *566*, 689–715.

Halliwell, J.V., and Adams, P.R. (1982). Voltage-clamp analysis of muscarinic excitation in hippocampal neurons. Brain Res. *250*, 71–92.

Hallworth, N.E., Wilson, C.J., and Bevan, M.D. (2003). Apamin-sensitive small conductance calcium-activated potassium channels, through their selective coupling to voltage-gated calcium channels, are critical determinants of the precision, pace, and pattern of action potential generation in rat subthalamic nucleus neurons in vitro. J. Neurosci. *23*, 7525–7542.

Harris, K.D., Hirase, H., Leinekugel, X., Henze, D.A., and Buzsaki, G. (2001). Temporal interaction between single spikes and complex spike bursts in hippocampal pyramidal cells. Neuron *32*, 141–149.

Hausser, M., Raman, I.M., Otis, T., Smith, S.L., Nelson, A., du Lac, S., Loewenstein, Y., Mahon, S., Pennartz, C., Cohen, I., and Yarom, Y. (2004). The beat goes on: spontaneous firing in mammalian neuronal microcircuits. J. Neurosci. *24*, 9215–9219.

Hoebeek, F.E., Stahl, J.S., van Alphen, A.M., Schonewille, M., Luo, C., Rutteman, M., van den Maagdenberg, A.M., Molenaar, P.C., Goossens, H.H., Frens, M.A., and De Zeeuw, C.I. (2005). Increased noise level of purkinje cell activities minimizes impact of their modulation during sensorimotor control. Neuron *45*, 953–965.

Hotson, J.R., and Prince, D.A. (1980). A calcium-activated hyperpolarization follows repetitive firing in hippocampal neurons. J. Neurophysiol. *43*, 409–419.

Hotson, J.R., Prince, D.A., and Schwartzkroin, P.A. (1979). Anomalous inward rectification in hippocampal neurons. J. Neurophysiol. *42*, 889–895.

Hu, H., Vervaeke, K., and Storm, J.F. (2002). Two forms of electrical resonance at theta frequencies, generated by M-current, h-current and persistent Na+ current in rat hippocampal pyramidal cells. J. Physiol. *545*, 783–805.

Kay, A.R., Sugimori, M., and Llinas, R. (1998). Kinetic and stochastic properties of a persistent sodium current in mature guinea pig cerebellar Purkinje cells. J. Neurophysiol. *80*, 1167–1179.

Koch, C. (1999). Biophysics of Computation: Information Processing in Single Neurons (Oxford: Oxford University Press), 156–157.

Lanthorn, T., Storm, J., and Andersen, P. (1984). Current-to-frequency transduction in CA1 hippocampal pyramidal cells: slow prepotentials dominate the primary range firing. Exp. Brain Res. *53*, 431–443.

Lien, C.C., and Jonas, P. (2003). Kv3 potassium conductance is necessary and kinetically optimized for high-frequency action potential generation in hippocampal interneurons. J. Neurosci. *23*, 2058–2068.

Lipowsky, R., Gillessen, T., and Alzheimer, C. (1996). Dendritic Na+ channels amplify EPSPs in hippocampal CA1 pyramidal cells. J. Neurophysiol. *76*, 2181–2191.

Madison, D.V., and Nicoll, R.A. (1984). Control of the repetitive discharge of rat CA 1 pyramidal neurones in vitro. J. Physiol. *354*, 319–331.

Magistretti, J., and Alonso, A. (1999). Biophysical properties and slow voltage-dependent inactivation of a sustained sodium current in entorhinal cortex layer-II principal neurons: a whole-cell and single-channel study. J. Gen. Physiol. *114*, 491–509.

Markram, H., Lubke, J., Frotscher, M., and Sakmann, B. (1997). Regulation of synaptic efficacy by coincidence of postsynaptic APs and EPSPs. Science *275*, 213–215.

Migliore, M., Hoffman, D.A., Magee, J.C., and Johnston, D. (1999). Role of an A-type K+ conductance in the back-propagation of action potentials in the dendrites of hippocampal pyramidal neurons. J. Comput. Neurosci. *7*, 5–15.

Nolan, M.F., Malleret, G., Lee, K.H., Gibbs, E., Dudman, J.T., Santoro, B., Yin, D., Thompson, R.F., Siegelbaum, S.A., Kandel, E.R., and Morozov, A. (2003). The hyperpolarization-activated HCN1 channel is important for motor learning and neuronal integration by cerebellar Purkinje cells. Cell *115*, 551–564.

Peters, H.C., Hu, H., Pongs, O., Storm, J.F., and Isbrandt, D. (2005). Conditional transgenic suppression of M channels in mouse brain reveals functions in neuronal excitability, resonance and behavior. Nat. Neurosci. *8*, 51–60.

Pinto, R.D., Elson, R.C., Szucs, A., Rabinovich, M.I., Selverston, A.I., and Abarbanel, H.D.I. (2001). Extended dynamic clamp: controlling up to four neurons using a single desktop computer and interface. J. Neurosci. Methods *108*, 39–48.

Sah, P., and Bekkers, J.M. (1996). Apical dendritic location of slow afterhyperpolarization current in hippocampal pyramidal neurons: implications for the integration of long-term potentiation. J. Neurosci. *16*, 4537–4542.

Sah, P., Gibb, A.J., and Gage, P.W. (1988). The sodium current underlying action potentials in guinea pig hippocampal CA1 neurons. J. Gen. Physiol. *91*, 373–398.

Schneidman, E., Freedman, B., and Segev, I. (1998). Ion channel stochasticity may be critical in determining the reliability and precision of spike timing. Neural Comput. *10*, 1679–1703.

Schreiber, S., Fellous, J.M., Tiesinga, P., and Sejnowski, T.J. (2004). Influence of ionic conductances on spike timing reliability of cortical

neurons for suprathreshold rhythmic inputs. J. Neurophysiol. *91*, 194–205.

Shao, L.R., Halvorsrud, R., Borg-Graham, L., and Storm, J.F. (1999). The role of BK-type Ca2+-dependent K+ channels in spike broadening during repetitive firing in rat hippocampal pyramidal cells. J. Physiol. *521*, 135–146.

Skaugen, E., and Walloe, L. (1979). Firing behaviour in a stochastic nerve membrane model based upon the Hodgkin-Huxley equations. Acta Physiol. Scand. *107*, 343–363.

Stafstrom, C.E., Schwindt, P.C., Chubb, M.C., and Crill, W.E. (1985). Properties of persistent sodium conductance and calcium conductance of layer V neurons from cat sensorimotor cortex in vitro. J. Neurophysiol. *53*, 153–170.

Storm, J.F. (1989). An after-hyperpolarization of medium duration in rat hippocampal pyramidal cells. J. Physiol. *409*, 171–190.

Storm, J.F. (1990). Potassium currents in hippocampal pyramidal cells. Prog. Brain Res. *83*, 161–187.

Stuart, G. (1999). Voltage-activated sodium channels amplify inhibition in neocortical pyramidal neurons. Nat. Neurosci. *2*, 144–150.

Stuart, G., and Sakmann, B. (1995). Amplification of EPSPs by axosomatic sodium channels in neocortical pyramidal neurons. Neuron *15*, 1065–1076.

Taddese, A., and Bean, B.P. (2002). Subthreshold sodium current from rapidly inactivating sodium channels drives spontaneous firing of tuberomammillary neurons. Neuron *33*, 587–600.

Traub, R.D., Jefferys, J.G., Miles, R., Whittington, M.A., and Toth, K. (1994). A branching dendritic model of a rodent CA3 pyramidal neurone. J. Physiol. *481*, 79–95.

Vogalis, F., Storm, J.F., and Lancaster, B. (2003). SK channels and the varieties of slow after-hyperpolarizations in neurons. Eur. J. Neurosci. *18*, 3155–3166.

Williams, S.R., Toth, T.I., Turner, J.P., Hughes, S.W., and Crunelli, V. (1997). The "window" component of the low threshold Ca2+ current produces input signal amplification and bistability in cat and rat thalamocortical neurones. J. Physiol. *505*, 689–705.

Wolfart, J., Neuhoff, H., Franz, O., and Roeper, J. (2001). Differential expression of the small-conductance, calcium-activated potassium channel SK3 is critical for pacemaker control in dopaminergic midbrain neurons. J. Neurosci. *21*, 3443–3456.